Electronic transport in degenerate (100) scandium nitride thin films on magnesium oxide substrates

John S. Cetnar,[1,a)] Amber N. Reed,[2] Stefan C. Badescu,[1] Shivashankar Vangala,[1] Hadley A. Smith,[2,3] and David C. Look[1,4]
[1]*Air Force Research Laboratory, Sensors Directorate, Wright Patterson AFB, Ohio 45433, USA*
[2]*Air Force Research Laboratory, Materials and Manufacturing Directorate, Wright Patterson AFB, Ohio 45433, USA*
[3]*Department of Physics, University of Dayton, Dayton, Ohio 45469, USA*
[4]*Semiconductor Research Center, Wright State University, Dayton, Ohio 45435, USA*

(Received 27 July 2018; accepted 25 October 2018; published online 8 November 2018)

Scandium nitride (ScN) is a degenerate n-type semiconductor with very high carrier concentrations, low resistivity, and carrier mobilities comparable to those of transparent conducting oxides such as zinc oxide. Because of its small lattice mismatch to gallium nitride (GaN), <1%, ScN is considered a very promising material for future GaN based electronics. Impurities are the source of the degeneracy. Yet, which specific impurities are the cause has remained in contention. ScN thin films of various thicknesses were grown on magnesium oxide substrates in a (001) orientation using reactive magnetron sputtering across a range of deposition conditions. X-ray diffraction was used to verify crystal orientation. Film thicknesses ranging from 39 to 85 nm were measured using scanning electron microscopy. The electronic transport properties of the films were characterized using Hall-effect measurements at temperatures ranging from 10 to 320 K. At 10 K, the electron concentration varies from 4.4×10^{20} to 1.5×10^{21} cm^{-3}, resistivity from 2.1×10^{-4} to 5.0×10^{-5} Ω·cm, and Hall mobility from 66 to 97 cm^2/V·s. Secondary ion mass spectroscopy (SIMS) was used to determine film compositions. Finally, density functional theory (DFT) was used to compute the activation energies for various point defects including nitrogen and scandium vacancies and oxygen and fluorine substituting for nitrogen. For both oxygen and fluorine substitution, the energies were negative, indicating spontaneous formation. Nevertheless, the combined results of the Hall, SIMS, and DFT strongly suggest that oxygen substitution is the primary mechanism behind the high carrier concentration in these samples. https://doi.org/10.1063/1.5050200

There have been many recent studies on the electronic and optical properties of scandium nitride.[1–8] From these studies, we know that ScN is an n-type semiconductor with a rock-salt structure. It has an indirect bandgap from Γ to X of 1.3 ± 0.3 eV.[3,9] Its lowest direct bandgap is 2.4 ± 0.3 eV at X.[3,9] The direct transition is commonly observed while the indirect transition is rare.[2] This is due to the small absorption cross-section of the indirect gap.[5] The lattice constant for ScN has been measured to be 0.4503 ± 0.0002 nm.[10–12] Therefore, when grown in the (111) orientation, the lattice mismatch between ScN and the c-plane of GaN is less than 1%.[3] ScN is nearly always degenerate, with electron concentration levels in the 10^{20}–10^{21} cm^{-3} range[1–3] and resistivities on the order of 10^{-5}–10^{-4} Ω·cm, close to those of metals. At these concentrations, ScN electron mobilities are lower than those reported in elemental and III-V compound semiconductors but are comparable to those seen in transparent conducting oxides such as zinc oxide.[13,14] To date, the highest room temperature (RT) mobility reported for epitaxially grown ScN is 284 cm^2/V·s by Oshima.[4] Typical RT thin film mobilities range between 30 and 100 cm^2/V·s for ScN at degenerate concentration levels. Decreasing the impurity concentration should reduce charge scattering and hence increase the mobility.[4] Dismukes *et al.*[10] speculated that if the ScN mobility were extrapolated to lower concentrations, ScN might have mobilities lying between those of Ge and Si. They further speculated that ScN could become a very useful material if lower doping could be achieved.[10] There are ongoing efforts aimed at realizing this goal today.[1,5] An open question in the study of ScN is: what is the dominant source of the high doping? Three candidates are mentioned most often in the literature: nitrogen vacancies (V_N^+),[4,8,9,15–17,20] oxygen substituting for nitrogen (O_N^+),[1,3,7,8,18–20] and fluorine substituting for nitrogen (F_N^+).[2,8,20] All of these impurities act as donors, with concentration levels varying with growth conditions. An identification of which is dominant under typical growth conditions is very important for a fundamental understanding of transport in ScN and in assessing theoretical limits of ScN based device performance. Further, if high mobility ScN is to be realized, then it seems like an attractive approach would be to reduce impurities during deposition, rather than add compensators. It is with this idea in mind that this research has approached the problem.

In this work, the electronic transport properties of ScN were studied using material growth, characterization, and theory. The goal was threefold: (1) grow high-quality ScN thin films; (2) accurately measure their compositions and electronic transport properties; and (3) use density functional theory (DFT) to investigate point defects and thereby identify the most likely sources of degeneracy.

ScN was deposited on (001) oriented magnesium oxide (MgO) using reactive magnetron sputtering in an ultra-high vacuum system with a base pressure of $\sim 10^{-9}$ Torr. A load

a)Author to whom correspondence should be addressed: john.cetnar.1@us.af.mil

lock system was used to introduce the substrates into the deposition chamber. Six films were grown, labelled RX-18 to RX-23, with target powers (W_T) varying from 25 to 200 W. During all growths, the total gas pressure was 20 mTorr, the nitrogen gas fraction was set to 75%, the coil current (which corresponded to an ion flux of $4.2 \times 10^{15}\,cm^{-2}{\cdot}s^{-1}$) was set to 4.00 A, and the substrate temperature was set to 550 °C. The deposition times, t, were scaled for each growth such that $W_T{\cdot}t$ was approximately constant. A summary of growth powers, growth times, thicknesses, deposition rate, (002) ScN coupled 2θ-ω x-ray diffraction (XRD) peak information, and lattice constants is given in Table I. The thicknesses were measured using cross-sectional scanning electron microscopy (SEM) and the deposition rate calculated from the thicknesses and deposition times. The lattice constants (a) were calculated from the XRD data. Rocking curve XRD scans of the MgO substrates show multiple domains with peaks at $\omega = 20.81°$, 20.88°, 20.92°, 21.01°, and 21.97°. The rocking curve XRD for the ScN films shows a single broad peak. The smallest full-width at half-maximum (FWHM) occurred for the sample grown at $W_T = 50$ W (RX-21) while the broadest FHWM was for RX-18 ($W_T = 200$ W). For all samples, the coupled 2θ-ω XRD scans (Fig. 1) show a single diffraction peak for ScN at $39.80° \pm 0.07°$ corresponding to (002)-oriented ScN. The 2θ position of the ScN peak shifts to higher diffraction angles as W_T is increased from 25 W to 75 W. Above 75 W, the diffraction angle decreased with higher W_T. The FWHM of the (002) diffraction peak also changed with sputter power. The sample grown with $W_T = 75$, RX-20, had the narrowest peak with a FWHM of 0.29°. The FWHM decreased with increasing sputter power until $W_T = 75$ W. Above 75 W, the FWHM increased with higher W_T. The coupled XRD scans suggest that all the samples are polycrystalline (002)-oriented ScN. Crystalline quality is dependent on sputtering power with sputter powers between 40 W and 75 W resulting in the best crystalline quality. The lattice constants for all the samples in this work are 0.44%–8.00% larger than the value of 4.500 Å for bulk ScN. Samples RX-20, 21, and 22 had lattice constants closest to the bulk value, with $a = 4.520$.

The electronic transport properties of the ScN thin films were measured using a Lakeshore 7507 Hall-effect measurement system. Temperature dependent Hall-effect measurements were made from 7 to 320 K, using a 20 mA excitation current, and an applied magnetic field, ±10 kG. The results for the measured carrier concentration (n), resistivity (ρ), and Hall mobility (μ_H) are shown in Fig. 2. The volume carrier concentrations and resistivities are based on the thicknesses measured by SEM (see Table I). In all cases, these concentrations as a function of measurement temperature are quite flat. However, mobilities decrease with temperature due to polar optical phonon scattering, and thus, resistivities must increase since $\rho = 1/(en\mu)$. This is typical metal-like behavior and quantitative analysis is straightforward. With respect to growth power, we note a strong trend. The highest powers, which resulted in the poorest crystallinity, produce both low concentration and low mobility. For a degenerate semiconductor, at the lowest temperatures (no phonons), the mobility is predominantly determined by the ratio $(N_D - N_A)/(N_D + N_A) = (1 - K)/(1 + K)$, where N_D and N_A are the donor and acceptor concentrations, respectively, and $K = N_D/N_A$ is the compensation ratio. Thus, if μ is decreasing as power increases, K must be increasing. This would occur if N_A is increasing, and one possibility is increased Sc-vacancy production due to the higher sputter power resulting in more rapid growth and poorer crystallinity (and likely more defects). However, this speculation will require further study.

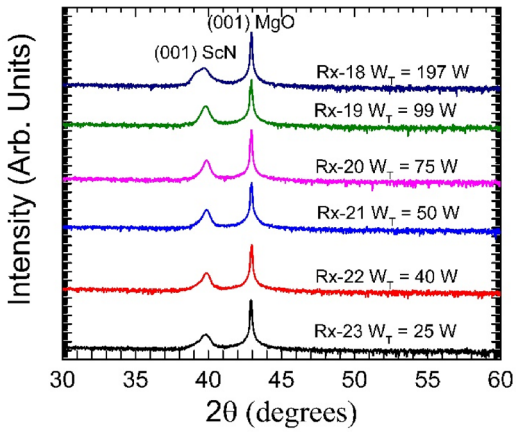

FIG. 1. Coupled 2θ–ω x-ray diffraction scans for ScN samples RX-18 through RX-23 grown on (001)-oriented MgO substrates with different sputter powers (W_T).

Secondary mass ion spectroscopy (SIMS) was performed on four of these samples (RX-18, RX-20, RX-21, and RX-23) by EAG Inc. SIMS was used to compare the relative Sc/N ratio and evaluate the oxygen (O) and fluorine (F) impurity profiles with depth. Within the SIMS margin of uncertainty (a few %), all of the samples were stoichiometric (i.e., Sc/N ≈ 1) or nearly so (slightly N-rich). From these

TABLE I. Growth power, growth time, sample thickness, deposition rate, (002)-ScN diffraction peak position, and FWHM from 2θ–ω scans and sample lattice constant for ScN samples RX-18 through RX-23.

Sample name	Power (W)	Time (min)	Thickness (nm)	Deposition rate (nm/min)	XRD 2θ peak position (°)	XRD 2θ peak FWHM (°)	Lattice constant a (Å)
RX-18	197	5	84	17	39.69	0.55	4.540
RX-19	99	10	64	6.4	39.74	0.33	4.526
RX-20	75	15	64	4.3	39.87	0.29	4.520
RX-21	50	20	48	2.4	39.86	0.32	4.520
RX-22	40	25	42	1.7	39.85	0.35	4.520
RX-23	25	40	39	1.0	39.79	0.46	4.525

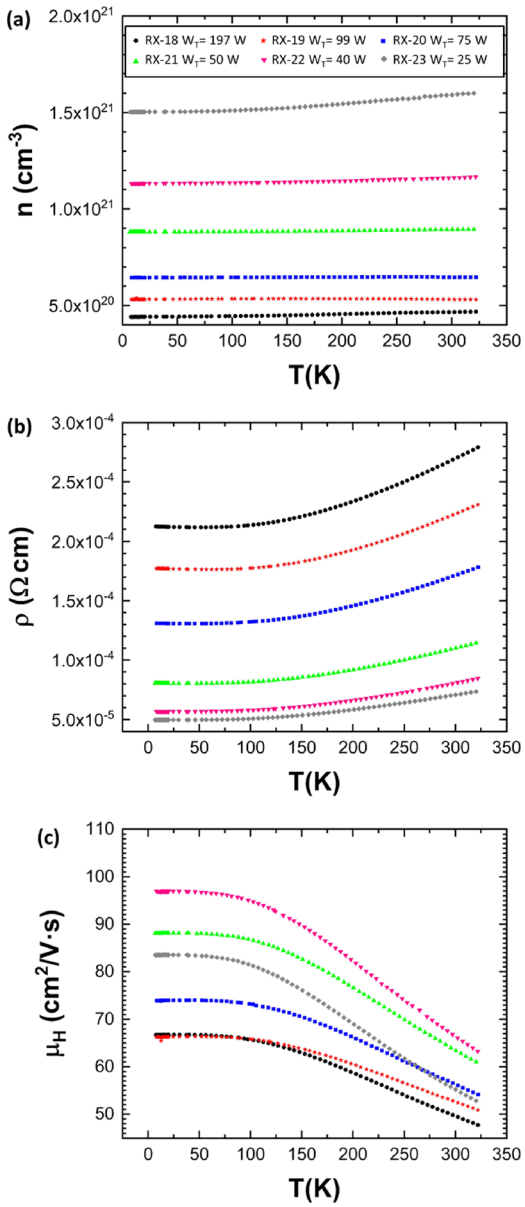

FIG. 2. (a) Measured carrier concentration, (b) resistivity, (c) and Hall mobility versus temperature for ScN samples RX-18 through RX-23.

measurements, it is difficult to estimate a quantity such as V_N. Figure 3 shows the O and F profiles versus depth. The data were calibrated using archived relative sensitivity factors (RSF) with an error estimate of 30%. The depths are uncalibrated. The data show significant O and F concentrations in all samples. The O impurity concentration is on the order of $10^{20}\,cm^{-3}$ for RX-18 and $10^{21}\,cm^{-3}$ for the other three samples and is fairly constant with depth for all samples. Meanwhile, the F impurity concentration is on the order of $10^{21}\,cm^{-3}$ for RX-18 near the surface but falls off sharply with depth. For the other three samples, F concentrations are on the order of $10^{19}\,cm^{-3}$ and fairly constant with depth. The primary source of the O is thought to be residual water vapor, O_2, CO_2, and CO remaining in the deposition chamber during growth.[5] The 99.99% pure target is thought to be the primary source of fluorine. According to the target supplier, the Sc meltstock used to create the target was dendritically formed from scandium fluoride (ScF_3). The fluorine in our samples is thought to be trace amounts left over in the Sc sputtering target after the purification processing.[2] The variation in the fluorine concentration with sputter power can be attributed to differences in the time available for accommodation and re-evaporation during film growth. The higher sputter power (i.e., 197 W) used for RX-18 results in a high deposition rate, R = 17 nm/min, which allows less time for the fluorine to escape the film surface before it is buried. This results in a larger concentration of fluorine being trapped in the film. The samples deposited with lower sputter powers had slower deposition rates, thus allowing more time for re-evaporation and a lower concentration of fluorine. Additionally, higher sputter powers result in more fluorine being sputtered from the target and available for incorporation in the ScN.

Density Function Theory (DFT) based first principles modeling was used to gain insight into the origin of doping in this material. We chose the Heyd-Scuzeria-Ernzernhof (HSE06) hybrid functional[21] to accurately model the bandgap of the pristine material and the projected-augmented wave method (PAW) for atomic pseudopotentials as implemented in the Vienna *Ab initio* Simulation Package (VASP).[22] The plane wave cutoff energy was 500 eV. For the pristine material, we obtained the direct bandgaps $E_g(\Gamma) = 3.73$ eV, $E_g(X) = 2.09$ eV, respectively, and an indirect bandgap $E_g(-\Gamma) = 0.95$ eV. The impurities were modeled using $4 \times 4 \times 4$ supercells corresponding to 64 Sc atoms and 64 N atoms and a uniform $4 \times 4 \times 4$ Brillouin-zone sampling configuration.

The calculated formation energies for native defects are shown in Fig. 4 and for selected N-substitutional donors in Fig. 5 for N-rich conditions. These include corrections for the finite size effects of the supercells,[23,24] such as image charge, electrostatic potential, and band filling correction. Among these, the former is the most important, since some of the defects have a large charge state (e.g., V_N^{+3} or V_{Sc}^{-3}) and the periodic charge interaction dominates. Accounting for this self-consistently[24] allows us to use the $4 \times 4 \times 4$ supercell size.

The DFT results show negative formation energies for both impurity defects O_N and F_N. Therefore, both form spontaneously in ScN. Meanwhile, native defects V_N and V_{Sc} have positive formation energies and do not form spontaneously (V_{Sc} is an acceptor). Formation energies for a variety of point defects have been communicated in a recent report.[8] While the formation energy for V_{Sc} agrees with our calculation, there is a difference for V_N: in Ref. 8, the transition point for V_N occurs above the conduction band minimum, and the lowest energy state is V_N^{+2} instead of V_N^{+3} as found by us. The former point is most likely due to a lower bandgap obtained in Ref. 8 with the standard HSE functional, while the latter is likely due to the precision in calculating paired hole states and band-filling corrections. These differences are much smaller than the difference between native defects and O_N and F_N found by us and do not change the main conclusion from our calculations.

The DFT results for n-type degenerate ScN indicate that O_N and F_N are much more likely to form than V_N. Although, as stated earlier, we cannot experimentally determine V_N from SIMS stoichiometry measurements, nevertheless, in the presence of significant quantities of O and/or F, we would

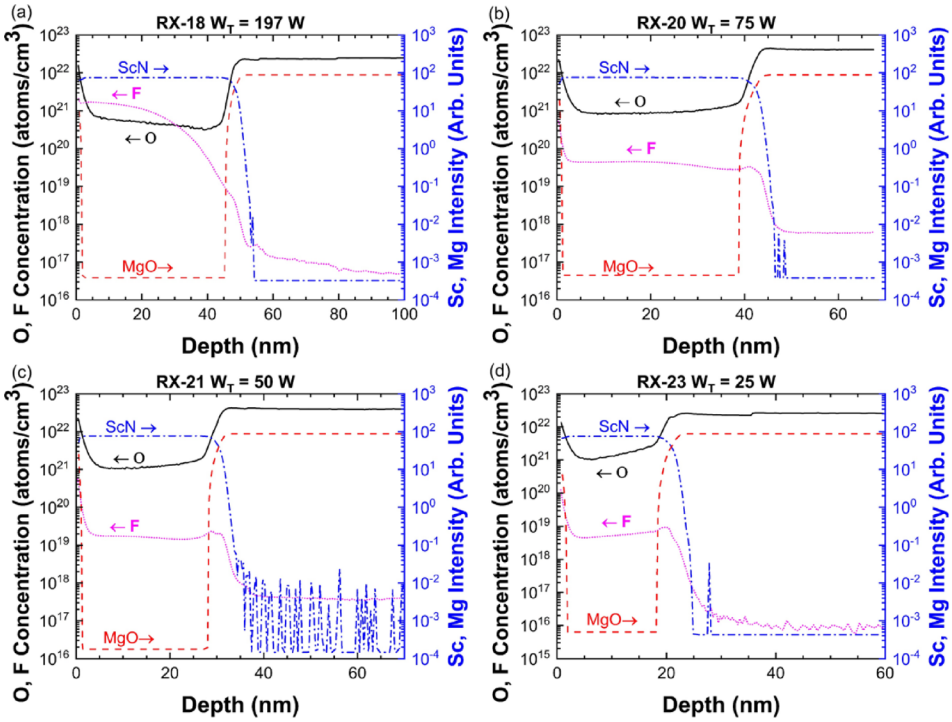

FIG. 3. SIMS measurement of O and F in (a) RX-18, (b) RX-20, (c) RX-21, and (d) RX-23.

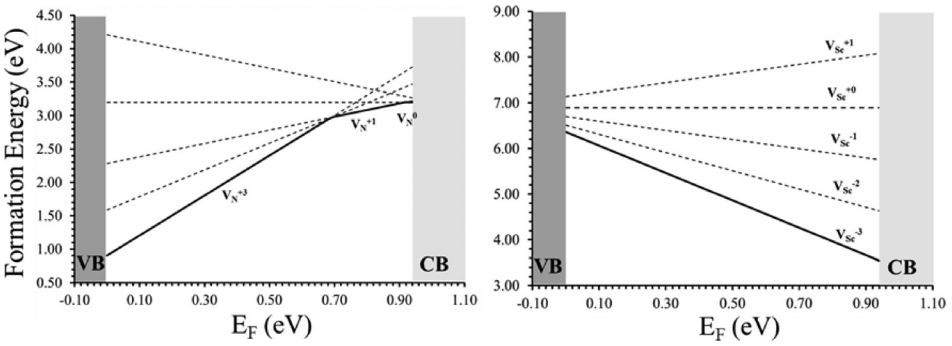

FIG. 4. Calculated formation energies for native defects (vacancies) in ScN for N-rich conditions.

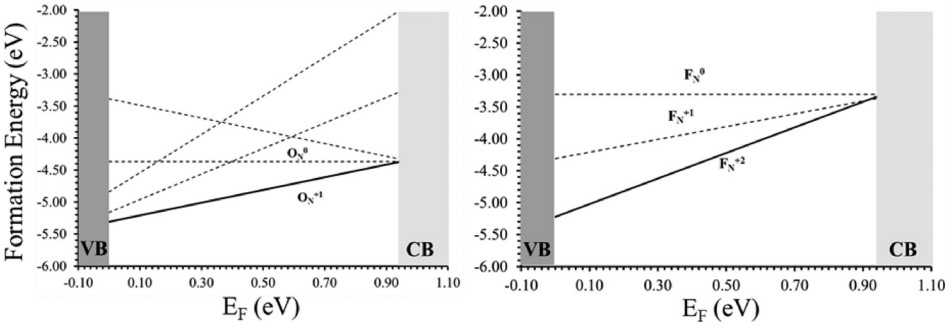

FIG. 5. Formation energies for substitutional donors in ScN for N-rich conditions.

expect one of them to be the dominant donor. Moreover, O_N has lower formation energy than F_N, so it is the more likely of the two to form. SIMS shows that oxygen is present in our samples at very high concentration levels, from 10^{20} to 10^{21} cm^{-3}. For all samples except RX-18, oxygen is 10–100 times more plentiful than fluorine. Finally, Hall-effect measurements indicate that the carrier concentrations are similar to the oxygen impurity concentrations and much greater than the fluorine concentrations (there is not nearly enough fluorine to account for all of the free carriers). Thus, the combination of results from Hall-effect measurements, SIMS measurements, and DFT calculations strongly suggest that oxygen substitution for nitrogen is the primary source of the high concentrations in our ScN samples.

The authors would like to thank T. A. Cooper for performing the Hall-effect measurements. This research was supported by the Air Force Office of Scientific Research through Project No. FA9550-RY17COR490. Also, H.A.S. was partially supported by the Southwestern Ohio Council for Higher Education and D.C.L. by NSF Grant No. DMR-1800130 (T. Paskova).

[1]B. Saha, M. Garbrecht, J. A. Perez-Taborda, M. H. Fawey, Y. R. Koh, A. Shakouri, M. Martin-Gonzalez, L. Hultman, and T. D. Sands, Appl. Phys. Lett. **110**, 252104 (2017).
[2]R. Deng, B. D. Ozsdolay, P. Y. Zheng, S. V. Khare, and D. Gall, Phys. Rev. B **91**, 045104 (2015).
[3]S. W. King, R. F. Davis, and R. J. Nemanich, J. Vac. Sci. Technol., A **32**, 061504 (2014).
[4]Y. Oshima, E. G. Villora, and K. Shimamura, J. Appl. Phys. **115**, 153508 (2014).
[5]B. Saha, G. Naik, V. P. Drachev, A. Boltasseva, E. E. Marinero, and T. D. Sands, J. Appl. Phys. **114**, 063519 (2013).
[6]T. Ohgaki, K. Watanabe, Y. Adachi, I. Sakaguchi, S. Hishita, N. Ohashi, and H. Haneda, J. Appl. Phys. **114**, 093704 (2013).
[7]M. A. Moram, Z. H. Barber, and C. J. Humphreys, Thin Solid Films **516**, 8569 (2008).
[8]Y. Kumagai, N. Tsunoda, and F. Oba, Phys. Rev. Appl. **9**, 034019 (2018).
[9]D. Gall, M. Stadele, K. Jarrendahl, I. Petrov, P. Desjardins, R. Haasch, T. Lee, and J. Greene, Phys. Rev. B **63**, 125119 (2001).
[10]J. P. Dismukes, W. M. Yim, and V. S. Ban, J. Cryst. Growth **13/14**, 365 (1972).
[11]M. A. Moram, Z. H. Barber, C. J. Humphreys, T. B. Joyce, and P. R. Chalker, J. Appl. Phys. **100**, 023514 (2006).
[12]D. Gall, M. Stoehr, and J. Greene, Phys. Rev. B **64**, 174302 (2001).
[13]U. Ozgur, Y. I. Alivov, C. Liu, A. Teke, M. A. Reshchikov, S. Dogan, V. Avrutin, S. J. Cho, and H. Markov, J. Appl. Phys. **98**, 041301 (2005).
[14]D. C. Look, D. C. Reynolds, J. R. Sizelove, R. L. Jones, C. W. Litton, G. Cantwell, and W. C. Harsch, Solid State Commun. **105**, 399 (1998).
[15]H. A. H. AL-Brithen, E. M. Trifan, D. C. Ingram, A. R. Smith, and D. Gall, J. Cryst. Growth **242**, 345 (2002).
[16]A. R. Smith, H. A. H. AL-Brithen, and D. C. Ingram, J. Appl. Phys. **90**, 1809 (2001).
[17]C. Stampfl, R. Asahi, and A. J. Freeman, Phys. Rev. B **65**, 161204(R) (2002).
[18]X. Bai, D. M. Hill, and M. E. Kordesch, Mater. Res. Soc. Symp. Proc. **572**, 529 (1999).
[19]P. V. Burmistrova, J. Maassen, T. Favaloro, B. Saha, S. Salamat, Y. R. Koh, M. S. Lundstrom, A. Shakouri, and T. D. Sands, J. Appl. Phys. **113**, 153704 (2013).
[20]S. Kerdsongpanya, N. V. Nong, N. Pryds, A. Zukauskait, J. Jensen, J. Birch, J. Lu, L. Hultman, G. Wingqvist, and P. Eklund, Appl. Phys. Lett. **99**, 232113 (2011).
[21]J. Heyd, G. E. Scuseria, and M. Ernzerhof, J. Chem. Phys. **118**(18), 8207 (2003).
[22]J. Hafner, J. Comput. Chem. **29**(13), 2044 (2008).
[23]S. Lany and A. Zunger, Phys. Rev. B **78**, 235104 (2008).
[24]C. Freysoldt, J. Neugebauer, and C. G. Van de Walle, Phys. Status Solidi B **248**(5), 1067 (2011).